Dynamics of Coupled Thermoacoustic Oscillators Under Asymmetric Forcing

Ankit Sahay,[*] Amitesh Roy, Samadhan A. Pawar, and R.I. Sujith

Department of Aerospace Engineering, Indian Institute of Technology Madras, Chennai 600036, India

Quenching of limit-cycle oscillations (LCOs), either through mutual coupling or external forcing, has attracted wide attention in several fields of science and engineering. However, the simultaneous utilization of these coupling schemes in quenching of LCOs has rarely been studied despite its practical applicability. We study the dynamics of two thermoacoustic oscillators simultaneously subjected to mutual coupling and asymmetric external forcing through experiments and theoretical modeling. We investigate the forced response of both identical and nonidentical thermoacoustic oscillators for two different amplitudes of LCOs. Under mutual coupling alone, identical thermoacoustic oscillators display the occurrence of partial amplitude death and amplitude death, whereas under forcing alone, asynchronous quenching of LCOs is observed at nonresonant conditions. When the oscillators are simultaneously subjected to mutual coupling and asymmetric forcing, we observe a larger parametric region of oscillation quenching than when the two mechanisms are utilized individually. This enhancement in the region of oscillation quenching is due to the complementary effect of amplitude death and asynchronous quenching. However, the forced response of coupled nonidentical oscillators shows that the effect of forcing is insignificant on attaining synchronization and quenching of oscillations in the oscillator that is not directly forced. Finally, we qualitatively capture the experimental results using a reduced-order theoretical model of two Rijke tubes that are coupled through dissipative and time-delay coupling and asymmetrically forced. We believe that these findings offer fresh insights into the combined effects of mutual and forced synchronization in a system of coupled nonlinear oscillators.

I. INTRODUCTION

Coupled interacting nonlinear oscillators appear extensively in physical systems around us [1]. Depending upon the nature of coupling, a population of interacting oscillators can synchronize starting from an initially incoherent or desynchronized state. Such synchronized oscillators can exhibit an emergence of ordered patterns as observed in several examples in nature, such as flocking of birds or flashing of light by fireflies [2]. However, synchronization of oscillations may be detrimental sometimes, and may need to be desynchronized [3] or quenched [4]. Here, we study the practical application of synchronization theory in attaining control of self-excited oscillations in a system of coupled prototypical thermoacoustic oscillators. A thermoacoustic oscillator refers to a confined combustion system (for example, gas turbine combustors and rocket engines). In such a system, positive feedback between the acoustic pressure oscillations and the heat release rate oscillations leads to the generation of large amplitude, self-sustained periodic oscillations in the acoustic field. The occurrence of these large-amplitude oscillations is referred to as thermoacoustic instability. The presence of such instabilities can inflict considerable damage to the mechanical and structural components used in gas turbine and rocket engines [5–7]. Complex interactions between the acoustic field, turbulent flow field, and heat release rate field has recently led to the widespread use of a complex systems approach to understand the phenomenon of thermoacoustic instability [6,8].

In general, there are two types of interactions leading to the synchronization of oscillators: mutual and forced [7]. In the former, oscillators mutually interact through bidirectional coupling, leading to the adjustment of phases and frequencies of both the oscillators to a common state of mutual synchronization. Oscillation quenching attained through the phenomenon of amplitude death (AD) in mutually coupled systems is an exciting prospect that has been shown to work for various systems [9–12]. Amplitude death in a population of strongly coupled oscillators refers to a situation where all the oscillators pull each other off of their oscillatory state into the same stable fixed point, leading to complete cessation of oscillations. If the mutual coupling is not strong enough, the situation of partial amplitude death (PAD) may arise, where some oscillators retain their oscillatory behavior while oscillations are

---

[*]ankitsahay02@gmail.com

ceased in others [13]. On the other hand, in the case of forced synchronization, an independent master system (an external force) drives a slave system (driven oscillator), thus forming a unidirectional master-slave system [14]. In this type of coupling, the driven system adjusts its phase and frequency to that of the external forcing during the state of synchronization. Depending upon the frequency and the amplitude of forcing, the natural oscillations can be phase locked to forcing, and in some cases, the self-excited oscillations can be completely suppressed through the phenomenon of asynchronous quenching [15,16].

Quite a few numerical studies have been conducted to investigate the simultaneous effect of forcing in a system of coupled oscillators. In a system of two weakly coupled Van der Pol oscillators, Battelino [17] observed that, when each oscillator is externally forced and a constant phase difference is present between the forcing signals applied to each of the oscillators, the system exhibits three-frequency quasiperiodicity. As the coupling strength and forcing amplitude are increased, three-frequency quasiperiodicity is first replaced by a two-frequency quasiperiodic regime, and subsequently by phase-locked periodic and chaotic regimes. The transition between the phase-locked region and the two- and three-frequency quasiperiodic regions takes place through saddle-node bifurcations [18,19]. The external force first destroys the regime of mutual synchronization of oscillators. As the forcing amplitude is increased, the oscillator that is subjected to external forcing synchronizes with the forcing signal first, followed by the forced synchronization of the entire system [20]. Similar observations were made in a system of coupled Van der Pol and Duffing oscillators [21]. Such an approach was utilized for modeling the effect of a pacemaker on the dynamics of the human heart [22]. On the flip side, only one experimental study has been conducted to understand the effect of forcing on mutually coupled electronic circuits with the aim of verifying the phase dynamics associated with regimes of desynchronized, mutually synchronized, two-frequency quasiperiodic, three-frequency quasiperiodic, and forced synchronized oscillations [18]. Furthermore, all the aforementioned studies focus on the phase dynamics of the system with particular attention afforded to the dynamics of bifurcations among quasiperiodic, periodic, and chaotic regimes. In light of the above discussed limitations of past studies, there is a need to experimentally quantify the effect of mutual coupling and external forcing on the amplitude of the limit-cycle oscillations (LCOs) observed in both the oscillators. Thus, we analyze the phase as well as the amplitude response of two coupled thermoacoustic oscillators under the condition of asymmetric external forcing, and model the observations with a low-order model. This makes up the key objective of the present study, and is of general interest to the nonlinear dynamics community.

Biwa *et al.* [4] experimentally demonstrated the control of LCOs through amplitude death in coupled thermoacoustic engines using both the dissipative and time-delay couplings. Thomas *et al.* [23] investigated amplitude death in a model of coupled Rijke tubes. They found that the simultaneous presence of dissipative and time-delay couplings was far more effective in attaining AD in the Rijke tubes than either of the two types of coupling applied separately. In a followup study with additive Gaussian white noise, Thomas *et al.* [24] observed that the presence of noise affects the coupled behavior of oscillators and mutual coupling only leads to about 80% suppression in the amplitude of the uncoupled LCOs as opposed to the state of AD observed in the absence of noise in the system. Dange *et al.* [25] performed detailed experimental characterization of coupled Rijke tube oscillators, and found that only time-delay coupling is sufficient to achieve AD of low-amplitude LCOs. In oscillators undergoing high-amplitude oscillations, frequency detuning is needed in addition to time-delay coupling for attaining AD and PAD. They also reported the phenomenon of phase-flip bifurcation in the coupling of identical thermoacoustic oscillators. Recently, Hyodo *et al.* [26] used a double-tube coupling method to significantly reduce the tube diameter necessary for demonstrating AD in a system of coupled identical Rijke tubes. Jegal *et al.* [27] demonstrated the occurrence of AD in a practical turbulent system consisting of two lean-premixed model swirl combustors. Moon *et al.* [28] compared the characteristics of mutual synchronization of these systems when the length and diameter of the coupling tube were changed. Jegal *et al.* [27] also found that, under different conditions, mutual synchronization can also trigger the strong excitation of a new mode, even when the two combustors are individually stable in the absence of coupling.

On the other hand, Balusamy *et al.* [29] experimentally studied the forced response of LCOs in a swirl-stabilized turbulent combustor using the framework of forced synchronization and observed different states such as phase locking, phase drifting, and phase trapping in the system. Kashinath *et al.* [30] highlighted the route to forced synchronization of limit-cycle, quasiperiodic, and chaotic oscillations in a numerical model of the premixed flame. These findings were verified in experiments on Rijke tubes [16] and laminar combustors [31–33]. Mondal *et al.* [16], Guan *et al.* [31], and Roy *et al.* [32] further showed that forcing at frequencies away from the natural frequency of LCOs lead to greater than an 80% decrease in their amplitude through a phenomenon known as asynchronous quenching.

The aforementioned studies demonstrate the possibility of controlling the thermoacoustic instability based on mutual or forced synchronization. However, the scope of these studies is still limited as external forcing can quench thermoacoustic instability in a single system in

a specific range of forcing parameters, whereas practical engines generally have multiple combustors working in tandem. Hence, information on how forcing of the thermoacoustic instability in one combustor affects the thermoacoustic instability developed in another combustor is still unknown. Similarly, mutual coupling works for two coupled oscillators; however, the parametric regime for which amplitude death is observed is limited. Therefore, there is a need to combine both these methodologies to overcome their individual limitations. Essentially, we aim to implement a proof of concept capable of combining the best of both strategies—asynchronous quenching and mutual synchronization—to control thermoacoustic oscillations. To this end, we couple two Rijke tubes during the state of thermoacoustic instability and subject one to external harmonic forcing (asymmetric forcing). We then measure the phase and amplitude response of the resulting acoustic pressure oscillations in the Rijke tubes at different conditions of forcing and coupling parameters. We perform asymmetric forcing experiments on identical and nonidentical thermoacoustic oscillators to comprehensively assess the response to forcing. We find that through asymmetric forcing, we can expand the region of oscillation quenching of thermoacoustic instability in the system of coupled identical Rijke tubes by compounding the effect of asynchronous quenching and mutual synchronization. Finally, we develop a model where two Rijke tube oscillators are coupled through dissipative and time-delay coupling and are forced asymmetrically. We show that the model compares favorably with the experimental results, indicating the usefulness of reduced-order modeling of coupled oscillator models under forcing.

The rest of the paper is organized as follows. In Sec. II we describe the experimental setup. In Sec. III A, we investigate the forced synchronization characteristics of a single Rijke tube. We then demonstrate the presence of AD and PAD in mutually coupled Rijke tubes in Sec. III B. In Sec. III C, we characterize the response of coupled identical Rijke tubes to asymmetric forcing. We consider the response of nonidentical oscillators in Sec. III D. In Sec. IV, we describe the model and numerically investigate the dynamics of coupled Rijke tube oscillators under forcing. Finally, we present the conclusions from the study in Sec. V.

II. EXPERIMENTAL SETUP

The experimental setup used in this study consists of a pair of horizontal Rijke tubes (Fig. 1). Rijke tube A has a cross section of 9.3×9.4 cm^2 with a length of 102 cm. Rijke tube B has a cross section of 9.3×9.5 cm^2 and a length of 104 cm. A decoupler of dimensions $102 \times 45 \times 45$ cm^3 is attached to the inlet of the respective Rijke tubes to eliminate upstream disturbances and ensure a steady flow in the system. Each Rijke tube consists of a separate
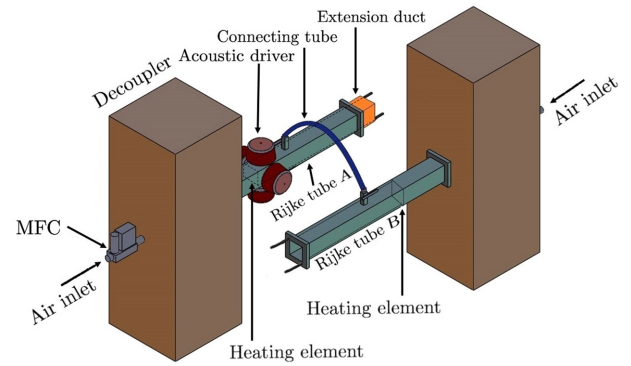

FIG. 1. Schematic of the experimental setup having two horizontal Rijke tube oscillators A and B, which are coupled using a connecting tube. Rijke tube A is acoustically forced with four acoustic drivers attached on its sides. An extension duct in Rijke tube A is used for implementing frequency detuning in the system.

electrically heated wire mesh, powered by an external dc power supply, which acts as a compact heat source. The heaters are located 27 cm downstream of the inlet in each duct. The air flow rate is maintained constant in each of the Rijke tubes through separate mass flow controllers (MFCs, Alicat Scientific) of uncertainty $\pm(0.8\%$ of the measured reading $+ 0.2\%$ of the full scale reading).

Both the Rijke tubes are coupled using a single vinyl tube of length L and internal diameter d (see Fig. 1). The ports for the connecting tube are located 57 cm downstream of the inlet. Ball-type valves are manually opened to establish coupling between the two oscillators. Four wall mounted acoustic drivers (Minsound TD-200A) are attached on each side of Rijke tube A, 41 cm downstream of the inlet. The acoustic drivers are connected in parallel to a power amplifier (Ahuja UBA-500M). Sinusoidal forcing signal with mean-to-peak amplitude (A_f, in millivolts mV) and frequency (f_f, in hertz Hz), generated using a Tektronix function generator (Model No. AFG1022) is input to the power amplifier to drive the coupled system.

A piezoelectric pressure transducer (PCB 103B02, sensitivity 217.5 mV/kPa, uncertainty ± 0.15 Pa) is mounted close to the midpoint along the length of the duct in each Rijke tube and is used for measuring the acoustic pressure fluctuations in the system. Data are acquired simultaneously from both the Rijke tubes at a sampling rate of 10 kHz for a duration of 5 s for each parametric condition using a data acquisition system (NI USB 6343). The resolution of frequency in the power spectrum of the signals is equal to 0.2 Hz. The rate of decay of an acoustic pulse generated from loudspeakers in the absence of flow is used to measure the damping in the two Rijke tubes. The acoustic decay rate values for Rijke tubes A and B are measured to be 16.5 ± 2 s^{-1} and 12.9 ± 1.8 s^{-1}, respectively. To ensure repeatability of the results and consistency of the

experimental conditions, the experiments are conducted only when the measured acoustic decay rates lie in the range mentioned above. A change in the decay rate only changes the critical parameter values at which the different dynamical states are observed; however, the overall dynamics remain the same. During each experiment, both the Rijke tubes are preheated for 10 min by supplying dc power at 1 V to the wire mesh. The preheating ensures a steady temperature profile inside the Rijke tubes.

A telescopic slide mechanism of 12 cm length is used to vary the length of Rijke tube A. The natural frequency of Rijke tube A can be varied between $f_{n0} = 162$ to 148 Hz with an uncertainty of ± 2 Hz due to the uncertainty in measuring the length of the Rijke tube. After preheating both the Rijke tubes, the heater power is increased such that the system undergoes subcritical Hopf bifurcation. The heater power is maintained away from the bistable region in all experiments. LCOs are maintained in each of the Rijke tubes before coupling is induced. The amplitude of the LCOs are controlled by varying the heater power and the air flow rate. All the experiments are reported for two different amplitudes (root mean square) of the LCOs in both the Rijke tubes in the uncoupled state: (a) lower amplitude $p_0' = 120$ Pa maintained by supplying a constant air flow rate of 2.4 ± 0.01 g/s (Re = 1370) in each Rijke tube, and (b) higher amplitude $p_0' = 200$ Pa maintained by supplying a constant air flow rate of 3.95 ± 0.01 g/s (Re = 2284) in each Rijke tube. After both the oscillators exhibit LCOs in their uncoupled state, the valves are opened to couple these oscillators. The coupled system is then asymmetrically forced through the loudspeakers connected to Rijke tube A.

III. RESULTS AND DISCUSSION

A. Response of a thermoacoustic oscillator to external forcing

We begin by investigating the forced acoustic response of LCOs in a single Rijke tube. In Fig. 2 we show a two-parameter bifurcation plot on an $\bar{A}_f$-f_f plane illustrating the phase [Figs. 2(a) and 2(c)] and amplitude [Figs. 2(b) and 2(d)] response of the LCOs under external forcing. The natural frequency of the LCOs is fixed at $f_{n0} = 160 \pm 2$ Hz. The forced response is studied for two different amplitudes of unforced LCOs: $p_0' = 120$ Pa, corresponding to $p_0 = 26$ mV [Figs. 2(a) and 2(b)], and $p_0' = 200$ Pa, corresponding to $p_0 = 43$ mV [Figs. 2(c) and 2(d)]. Here, p_0' refers to the amplitude of the unforced LCOs in pascal (Pa), and p_0 refers to the equivalent reading obtained from the piezoelectric transducer in millivolts. The values of the forcing amplitude A_f (in millivolts) are normalized with the unforced amplitude of LCOs measured in millivolts such that $\bar{A}_f = A_f / p_0$.

In Figs. 2(a) and 2(c), we plot the distribution of the phase locking value (Φ) between the forced LCOs and the

external forcing signal in the $\bar{A}_f$-f_f plane. A phase locking value quantifies the degree of synchronization between a pair of oscillators at any given condition of forcing (A_f, f_f). It is defined as [7]

$$\Phi = \frac{1}{N} \left| \sum_{n=1}^{N} \exp(i\Delta\phi) \right|, \quad (1)$$

where N is the length of the p' signal and $\Delta\phi$ is the instantaneous phase difference between the p' and forcing signals. Here, forcing is assumed to be sinusoidal of the form $F(t) = A_f \sin(2\pi f_f t)$. The instantaneous phase of the signals is determined using the analytic signal approach utilizing the Hilbert transform [7]. A Φ of 1 indicates synchronization of two oscillators, while a Φ of 0 indicates desynchronization of the oscillators. In experimental situations, it is difficult to obtain $\Phi = 1$; hence, we denote phase synchronization boundaries of LCOs through a least-square fit of the points where $\Phi = 0.98$. The R^2 values of the least-square-fit lines are given in Sec. I of the Supplemental Material [34]. The V-shaped region, called the Arnold tongue, separates the region of forced synchronization from the region of desynchronization. We note that the critical amplitude of forcing required for forced synchronization of LCOs, $A_f = A_{f,c}$, increases almost linearly with an increase in the frequency difference $\Delta f = |f_f - f_{n0}|$.

From Figs. 2(a) and 2(c) we note that, for $p_0' = 200$ Pa, the range of f_f for which forced synchronization occurs in the system is smaller than that observed for $p_0' = 120$ Pa, indicating the dependence of forced synchronization of LCOs on their amplitude in the unforced state. Furthermore, at higher values of Δf, achieving forced synchronization of both LCOs becomes difficult. We also observe regions of desynchronized oscillations (indicated in red) in the range of $f_f / f_{n0} = 0.62 - 0.70$ at high values of $\bar{A}_f$ [i.e., for $\bar{A}_f > 0.35$ in Figs. 2(a) and 2(c)]. The reason for desynchrony in this region is a result of period-3 behavior in p', which leads to low values of Φ (see Sec. II of the Supplemental Material [34]).

We also plot the normalized change in the amplitude of LCOs due to external forcing, $\Delta p'_{\text{rms}}/p_0' = (p_0' - p'_{\text{rms}})/p_0'$ in Figs. 2(b) and 2(d). Here, $\Delta p'_{\text{rms}}/p_0' \sim 1$ corresponds to complete suppression of LCOs in the Rijke tube due to forcing, whereas $\Delta p'_{\text{rms}}/p_0' < 0$ indicates an increase in the amplitude of LCOs above the unforced value due to forcing. The green region in Figs. 2(b) and 2(d) corresponds to an increase in the amplitude of LCOs above twice of its unforced value (i.e., $\Delta p'_{\text{rms}}/p_0' < -1$) due to resonant amplification of the acoustic pressure signal as f_f is very close to f_{n0}. The simultaneous occurrence of forced synchronization for $f_f \approx f_{n0}$ along with the resonant amplification of the amplitude of LCOs is referred to as synchronance [16]. We further observe a large region with a reduction in amplitude greater than 80% of p_0' only
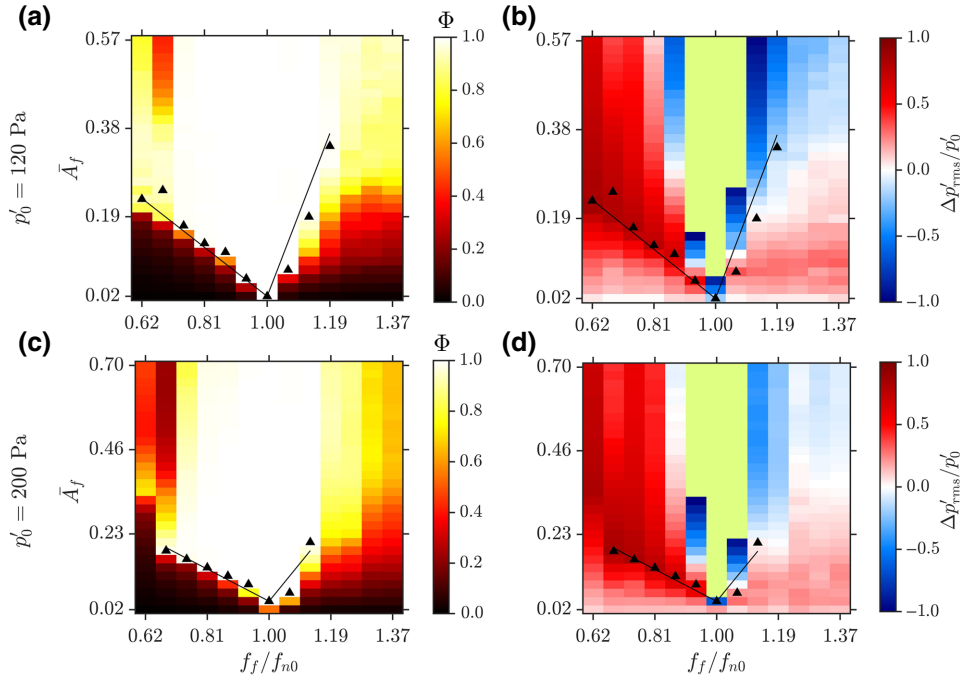
FIG. 2. Forced response of a single Rijke tube. (a),(c) The phase response shown in terms of the PLV and (b),(d) the amplitude response in terms of the fractional change in the amplitude of LCOs in the Rijke tube for (a),(b) $p'_0 = 120$ Pa and (c),(d) $p'_0 = 200$ Pa for different values of $\bar{A}_f$ and f_f. The synchronization boundaries in (a)–(d) are obtained through a least-square fit of points where $\Phi = 0.98$. The R^2 values for the least-square fitting are given in Sec. I of the Supplemental Material [34]. (a),(c) The region of forced synchronization decreases with increasing p'_0 (b),(d) while quenching of LCOs is observed only for $f_f < f_{n0}$. Green region around $f_f/f_{n0} = 1$ in (b),(d) signifies the amplification of LCOs above twice the value of the unforced amplitude, such that $\Delta p'_{rms}/p'_0$ varies in the range $(-5.76, -1)$ in (b) and $(-4.47, -1)$ in (d).

for $f_f < f_{n0}$ [16]. A significant decrease in the amplitude of LCOs at nonresonant conditions ($f_f \neq f_{n0}$) of forcing is a result of asynchronous quenching [16,31]. Asynchronous quenching of LCOs is achieved through forced synchronization, where the response p' signal oscillates at f_f, which can be seen from the coincidence of the boundaries of the Arnold tongue with region corresponding to $\Delta p'_{rms}/p'_0 \approx 1$ [see Figs. 2(b) and 2(d)]. The asymmetry in the characteristics of the Arnold tongue and asynchronous quenching of LCOs arises due to the inherent nonlinearity of the thermoacoustic system [30,32].

B. Response of coupled thermoacoustic oscillators

We now examine the response of two mutually coupled Rijke tubes when the length of the coupling tube (L) and the frequency detuning Δf_{n0} ($= f^B_{n0} - f^A_{n0}$) between them are varied independently, where f^A_{n0} and f^B_{n0} are the natural frequencies of oscillators A and B in the uncoupled state, respectively. In this study, the diameter of the connecting tube is kept constant at 1 cm for all the experiments (see Sec. III of the Supplemental Material [34]).

We note that the use of the connecting tube induces an acoustic time delay in the coupling between the two

Rijke tubes, as a finite time is required for the acoustic waves in the two oscillators to interact with one another [25]. A change in the length of the coupling tube changes the acoustic time delay between the two mutually interacting Rijke tubes. A change in the diameter of the coupling tube possibly changes the coupling strength between the two interacting Rijke tubes. The coupling strength comprises of two parts: time-delay coupling and dissipative coupling. Dissipative coupling of oscillators is related to their interaction arising due to the mass transfer via a connecting tube and also the acoustic loss occurring in the connecting tube [35]. We observe the presence of both time-delay and dissipative coupling in our system.

In Fig. 3, we plot the fractional change in the amplitude of LCOs in these oscillators, $\Delta p'_{rms}/p'_0$, as a function of L and Δf_{n0} for two different values of $p'_0 = 120$ Pa [Figs. 3(a) and 3(b)] and 200 Pa [Figs. 3(c) and 3(d)]. The color bar illustrating $\Delta p'_{rms}/p'_0$ values range from 0 to 1. During mutual coupling of oscillators, we seldom observe any amplification of LCOs. As a result, $\Delta p'_{rms}/p'_0$ is never negative. In contrast, during forcing experiments in Figs. 2(b) and 2(d), we observe resonant amplification of LCOs.
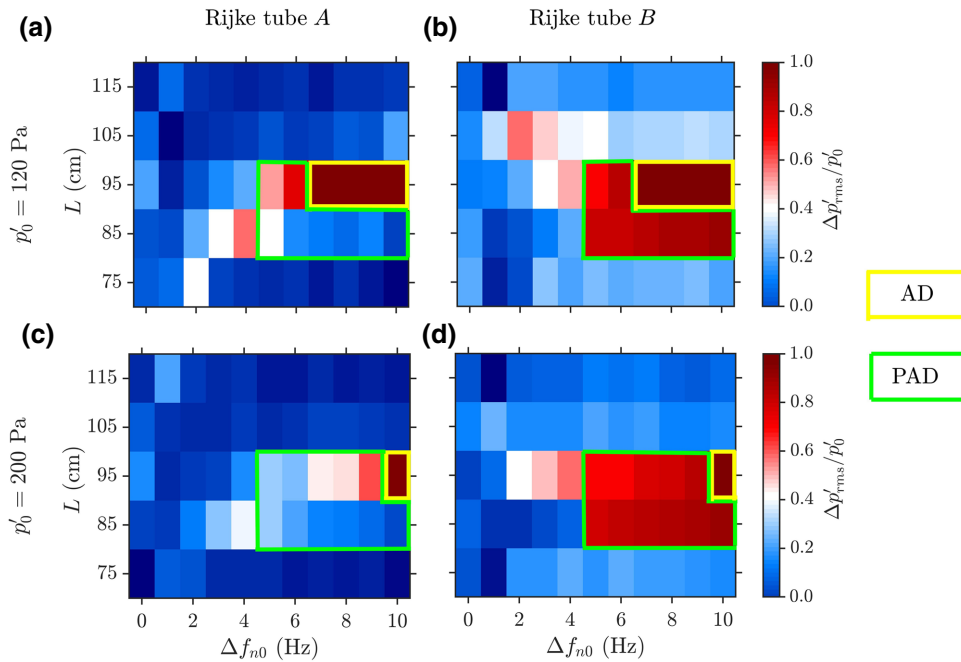
FIG. 3.   Coupled response of two Rijke tubes. Fractional change in the amplitude of LCOs for Rijke tubes A and B as functions of the frequency detuning ($\Delta f_{n0} = |f_{n0}^A - f_{n0}^B|$) and length of the connecting tube (L) for (a),(b) $p_0' = 120$ Pa and (c),(d) $p_0' = 200$ Pa in both the oscillators. The regions of AD and PAD are indicated. At other regions in the plots, LCOs are observed at reduced amplitude due to coupling. The parametric region exhibiting AD shrinks in size as p_0' is increased from 120 to 200 Pa.

In Fig. 3, for identical oscillators ($\Delta f_{n0} = 0$ Hz), we do not observe any perceivable reduction in the amplitude of LCOs due to coupling for either values of p_0'. However, a significant reduction in the amplitude of LCOs is observed when nonidentical oscillators (i.e., $f_{n0}^A \neq f_{n0}^B$) are coupled. We observe two states of oscillation quenching, i.e., AD and PAD, in coupled Rijke tubes for a particular range of L. For example, when $\Delta f_{n0} = 5$–10 Hz and $L = 85$ cm, we witness the presence of PAD in the system (see the green box in Fig. 3), while for $\Delta f_{n0} = 7$–10 Hz and $L = 95$ cm, we note the occurrence of AD in the system (see the yellow box Fig. 3). During the state of PAD, LCOs in Rijke tube B (unforced) undergo suppression and those in Rijke tube A (forced) remain at the reduced amplitude. For the state of AD, we observe greater than a 95% decrease in the amplitude of LCOs in both the oscillators due to coupling. The range of Δf_{n0} for which AD is observed in the system is smaller for $p_0' = 200$ Pa [Figs. 3(c) and 3(d)] when compared to that for $p_0' = 120$ Pa [Figs. 3(a) and 3(b)]. Thus, the occurrence of AD in Rijke tube oscillators has a dependence on the amplitude of uncoupled LCOs. It is quite clear from Fig. 3 that the mutual coupling induced through the coupling tube is not capable of inducing AD in identical oscillators, and the occurrence of AD in high-amplitude LCOs is restricted to a small range of L and requires a finite value of Δf_{n0} in the system [25].

C. Response of coupled identical thermoacoustic oscillators under asymmetric forcing

As observed in Fig. 3, in the absence of frequency detuning, mutual coupling is ineffective in achieving oscillation quenching (i.e., AD or PAD) in the coupled system. Hence, we asymmetrically force the coupled thermoacoustic oscillators to enhance the quenching of LCOs. In Fig. 4 we show the representative time series of the acoustic pressure fluctuations in Rijke tubes A (in blue) and B (in brown) under the effect of mutual coupling and external forcing when introduced sequentially. Both the oscillators are initially coupled through a single tube and then oscillator A is forced through loudspeakers. The time instant when coupling and forcing are switched on and off are marked as well. In some situations, we note that coupling and forcing can marginally reduce the amplitude of LCOs in the coupled system [Fig. 4(a)]. While in others, forcing can completely quench LCOs in one and reduce the amplitude of LCOs in the other oscillator [Fig. 4(b)]. This situation is akin to the state of PAD. Thus, forcing aids in attaining PAD. On the flip side, in Fig. 4(c), we observe that forcing can also lead to an amplification of the acoustic pressure oscillations, as can be seen from the increased amplitude of these oscillations in Rijke tube A above the uncoupled value. In contrast, the acoustic pressure oscillations remain quenched in Rijke tube B. Thus, the effectiveness of coupling and forcing of thermoacoustic oscillators is restricted
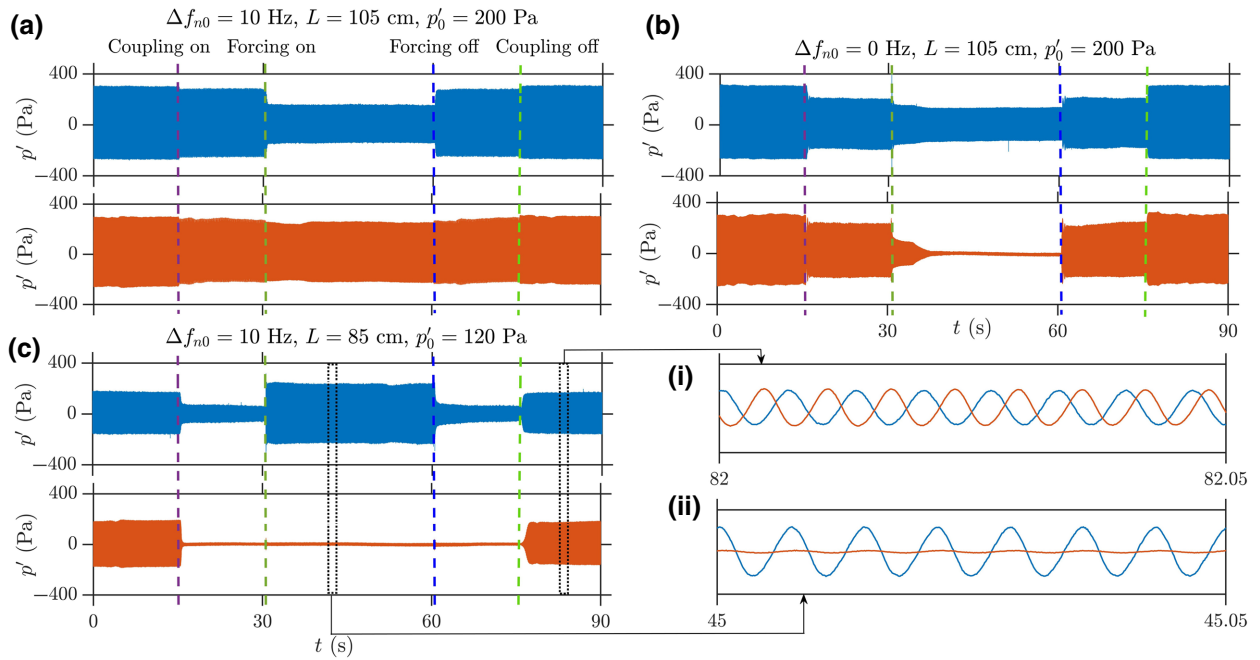
FIG. 4.　(a)–(c) Time series of p' in Rijke tubes A (blue) and B (brown) sequentially illustrating the effect of coupling and forcing on the amplitude of LCOs in both the Rijke tubes for different coupling and forcing parameters. In (a),(c), the Rijke tubes are nonidentical and have a frequency difference of 10 Hz. (i),(ii) The enlarged portions of the desynchronized LCOs and the state of PAD in (c), respectively. The coupling of oscillators always leads to a reduction in the amplitude of LCOs, while forcing of oscillators can have both reduction and amplification effects, depending on the values of the coupling and forcing parameters. The common parameters in all plots are $d = 10$ mm, $f_f = 140$ Hz, and $A_f = 30$ mV.

to a particular range of coupling and forcing parameters and, hence, we focus on the identification of such regions in the subsequent discussion.

In Fig. 5, we plot the amplitude [Figs. 5(a) and 5(b)] and the phase [Figs. 5(c) and 5(d)] response of identical Rijke tubes as functions of the forcing amplitude (A_f) and the length of coupling tube (L). The phase response is determined from the Φ calculated between the external forcing signal and p' for either of the Rijke tubes. Only Rijke tube A is subjected to external forcing. The forcing frequency is chosen as $f_f = 100$ Hz ($f_f/f_{n0} \approx 0.6$) for which we observe asynchronous quenching in a single forced Rijke tube oscillator [Fig. 2(d)].

For $A_f = 0$, we observe that a change in L does not lead to any suppression of LCOs in the oscillators [Figs. 5(a) and 5(b)]. With an increase in A_f, we observe a gradual decrease in the amplitude of LCOs in both the oscillators with the effect on Rijke tube B (unforced) being more pronounced than Rijke tube A (forced). Complete suppression of LCOs ($\Delta p'_{rms}/p'_0 \approx 1$) is observed in a particular range of L in Rijke tube B [Fig. 5(b)], while a significant decrease in the amplitude of LCOs (i.e., $\Delta p'_{rms}/p'_0 \approx 0.8$) is observed over a wider range of L in Rijke tube A [Fig. 5(a)]. For the coupled systems without forcing in Fig. 3, we did not observe AD or PAD when identical Rijke tubes are coupled for any L. However, the same coupled identical

oscillators when asymmetrically forced exhibit the state of PAD for a range of L [see point (e) in Fig. 5(a)]. Thus, we note that a larger region over which suppression of high-amplitude LCOs can be achieved in coupled identical thermoacoustic oscillators when the oscillators are coupled in a particular range of L and asymmetric forcing is applied at nonresonant frequencies. We reiterate that we do not observe complete suppression of the amplitude of LCOs in Rijke tube A.

Furthermore, we note that the region of quenching of LCOs in Rijke tube A [i.e., $p'_{rms}/p'_0 > 0.8$ in Fig. 5(a)] nearly coincides with the region of forced synchronization [i.e., $\Phi \approx 1$ in Fig. 5(c)], while the other regions remain desynchronized with the forcing signal. However, the LCOs in Rijke tube B always remain desynchronized with the forcing signal, which is observed from the value of $\Phi \sim 0$ in Fig. 5(d). For the regions where we do not observe suppression of LCOs in Rijke tube B, the difference between f_f and f_{n0} is too large such that there is no phase locking between oscillations in Rijke tube B and the forcing signal, resulting in low values of Φ. For the regions where we find complete suppression in Rijke tube B [Fig. 5(e)], the oscillations are noisy with very low amplitude, leading to low values of Φ.

The blue and red time series shown in Fig. 5(g) depict the acoustic pressure fluctuations in Rijke tubes A and B,
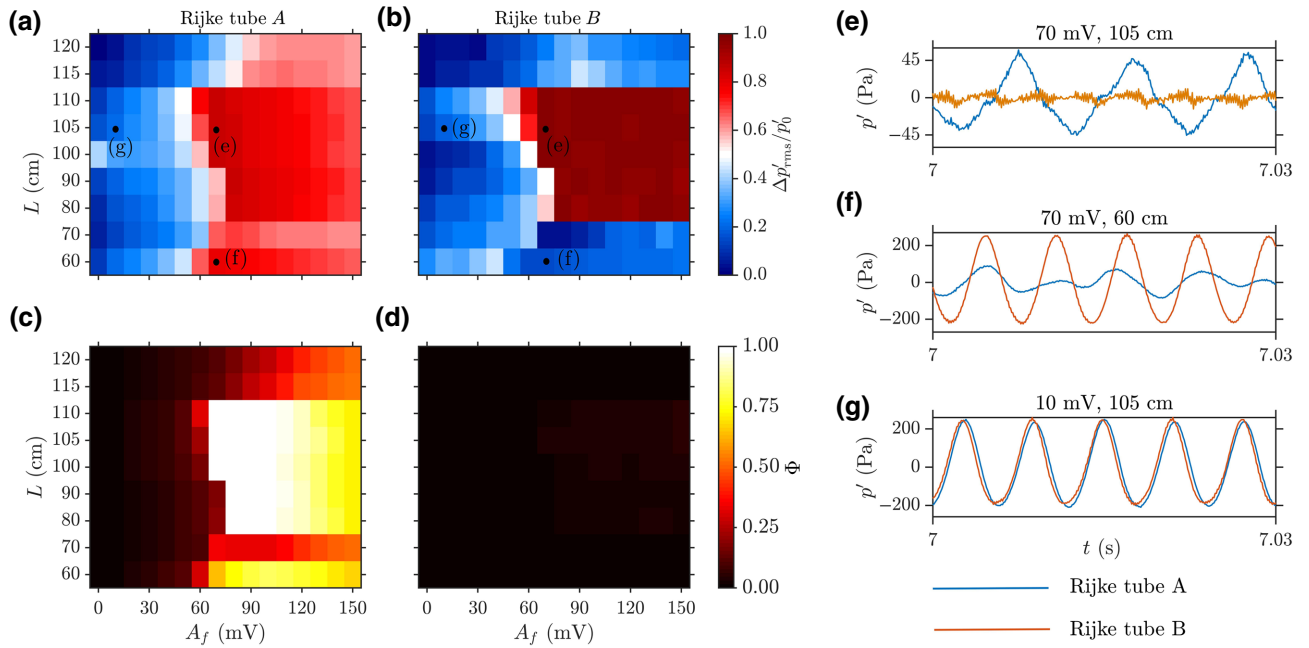
FIG. 5. Response of coupled, identical oscillators to asymmetric forcing. (a),(b) Amplitude and (c),(d) phase response as functions of the forcing amplitude (A_f) and length of the coupling tube (L). (e)–(g) Representative time series of p' for the points indicated in (a), depicting the difference in the response of Rijke tubes A and B. Complementary forcing and coupling enhances the region of L over which the suppression of LCOs is observed in both the oscillators. Forcing is ineffective in synchronization of LCOs in Rijke tube B [the black region in (d) denotes the complete desynchrony of LCOs in Rijke tube B with the forcing signal], while the region of quenching of LCOs in Rijke tube A nearly coincides with the region of forced synchronization ($\Phi \approx 1$). The common parameters in all the plots are $p'_0 = 200$ Pa, $f_f = 100$ Hz ($f_f/f_{n0} \approx 0.6$), $\Delta f_n = 0$ Hz, and $d = 1$ cm.

respectively, and the acoustic pressure time series correspond to data point (g) in Figs. 5(a) and 5(b). Although these signals appear mutual phase synchronized with each other in Fig. 5(g), they are desynchronized with the forcing signal due to a difference in the frequencies of their oscillations (i.e., $f_{n0} = 160$ Hz and $f_f = 100$ Hz). Therefore, the Φ distribution quantifying forced synchronization in Figs. 5(c) and 5(d) show zero values for data point (g).

Next, we measure the effect of forcing on the Arnold tongue and the amplitude quenching characteristics of the coupled identical Rijke tubes. The length and internal diameter of the coupling tube are fixed at $L = 105$ cm and $d = 1$ cm, respectively. Only Rijke tube A is forced externally. The natural frequency of both the oscillators is maintained at $f_{n0}^A = f_{n0}^B \approx 160$ Hz. In Fig. 6, we depict the fractional change in the amplitude of LCOs for each oscillator overlapped with the Arnold tongue in the $\bar{A}_f$-f_f plane for $p'_0 = 120$ Pa [Figs. 6(a) and 6(b)] and $p'_0 = 200$ Pa [Figs. 6(c) and 6(d)].

When the coupled Rijke tubes are asymmetrically forced, we note forced synchronization at a lower value of $\bar{A}_f$ for Rijke tube A than for Rijke tube B at any value of f_f. Therefore, the boundaries of the Arnold tongue are observed to be longer and the forced synchronization region is wider for Rijke tube A [Figs. 6(a) and 6(c)] than

that for Rijke tube B [Figs. 6(b) and 6(d)]. Furthermore, we note that the boundaries of the Arnold tongue for $p'_0 = 120$ Pa are less steep than those for $p'_0 = 200$ Pa. This means that a significantly larger value of the forcing amplitude is required to synchronize and quench the large-amplitude LCOs in the coupled Rijke tube oscillators. As the external forcing is applied to Rijke tube A, the region of resonant amplification is larger than that for Rijke tube B. Moreover, as the forcing amplitude is increased, the oscillator that is subjected to external forcing (i.e., Rijke tube A) synchronizes with the forcing signal first, followed by the forced synchronization of the entire system, i.e., the coupled system of Rijke tubes A and B. Furthermore, the transition from desynchronized to forced synchronization for Rijke tubes A and B takes place through a sequence of bifurcations: (i) from desynchronized limit cycle at $f_{n0}^{A,B}$ to two-frequency quasiperiodicity through torus-birth bifurcation ($f_{n0}^{A,B}, f_f$), and (ii) from two-frequency quasiperiodicity to synchronized limit cycle (f_f) either through saddle-node bifurcation if $f_{n0}^{A,B}$ is close to f_f or through torus-death bifurcation if $f_{n0}^{A,B}$ is far from f_f. These two routes are quite well known [14] and are observed for the identically coupled Rijke tubes under forcing. Here, f_{n0} denotes the natural frequency of the Rijke tubes in the uncoupled state.
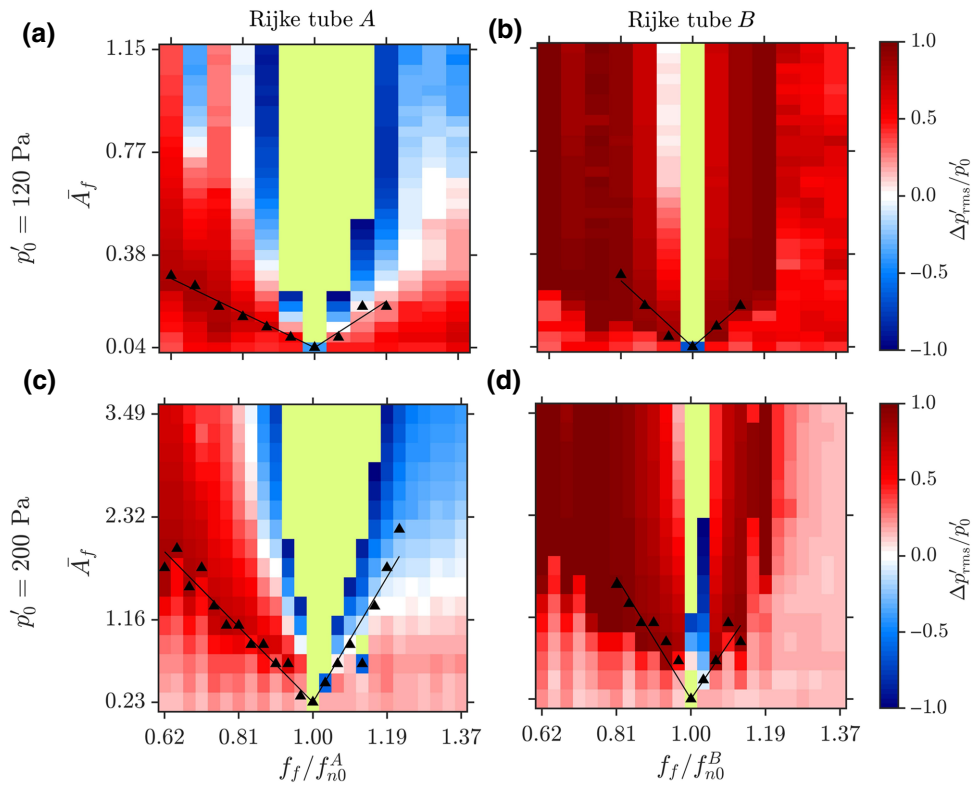
FIG. 6. Amplitude and phase response (black lines) of Rijke tubes A and B when coupled identical oscillators are subjected to asymmetric forcing for (a),(b) $p_0' = 120$ Pa and (c),(d) $p_0' = 200$ Pa. The LCOs in Rijke tube A are externally forced through the acoustic drivers. The forced synchronization region is wider for Rijke tube A than that observed for Rijke tube B, whereas a much larger magnitude of suppression of LCOs is observed in Rijke tube B as compared to that in Rijke tube A. Inside the green region, the oscillations are amplified to values above twice the value of the LCO amplitude in the uncoupled-unforced Rijke tubes, such that $\Delta p_{\mathrm{rms}}'/p_0'$ is observed in the range $(-6.47, -1)$ in (a), $(-3.54, -1)$ in (b), $(-6.67, -1)$ in (c), and $(-2.66, -1)$ in (d). Experimental conditions are $f_{n0}^A = f_{n0}^B \approx 160$ Hz, $L = 105$ cm, $d = 1$ cm.

Rijke tube A [Figs. 6(a) and 6(c)] shows a similar trend of quenching of different amplitude LCOs as observed for the single oscillator [Figs. 2(b) and 2(d)]. The similarities include an approximate coincidence of regions of maximum amplitude suppression with the synchronization boundary, significant amplitude suppression only for forcing frequencies of $f_f < f_{n0}$, and the presence of resonant amplification region around $f_f /f_{n0} \sim 1$ (shown in green). However, the $\bar{A}_f$ required for forced synchronization at any f_f for the coupled identical oscillators [Figs. 6(a) and 6(c)] is higher than that for a single oscillator [Figs. 2(b) and 2(d)].

In contrast to the response of Rijke tube A, the simultaneous effect of coupling and external forcing leads to a much greater suppression of LCOs along the boundaries of forced synchronization in Rijke tube B [Figs. 6(b) and 6(d)]. Suppression of LCOs in Rijke tube B is observed for both $f_f < f_{n0}$ and $f_f > f_{n0}$, unlike Rijke tube A where we note a reduction only for $f_f < f_{n0}$. Furthermore, the range of f_f and $\bar{A}_f$ over which the suppression of LCOs occurs in Rijke tube B is larger than that observed for

Rijke tube A. Thus, we reassert that an asymmetrically forced coupled system exhibits suppression of higher-amplitude LCOs for a larger range of forcing parameters than that observed when the oscillators are forced or coupled individually.

D. Forced response of coupled nonidentical limit-cycle oscillators

Now, we study the response of coupled nonidentical Rijke tubes under asymmetric forcing. Only Rijke tube A is externally forced. In Fig. 7, we depict the Arnold tongue and the fractional change in the amplitude of LCOs for $p_0' = 120$ Pa [Figs. 7(a) and 7(b)] and $p_0' = 200$ Pa [Figs. 7(c) and 7(d)]. The oscillators are coupled through a tube of $L = 105$ cm and $d = 1$ cm. A frequency detuning between the uncoupled oscillators is fixed at 10 Hz (i.e., $\Delta f_{n0} = f_{n0}^B - f_{n0}^A = 10$ Hz). We note that the effect of forcing is quite insignificant for synchronization of LCOs in Rijke tube B. We observe a small range of f_f (i.e., $f_f < f_{n0}^B$)
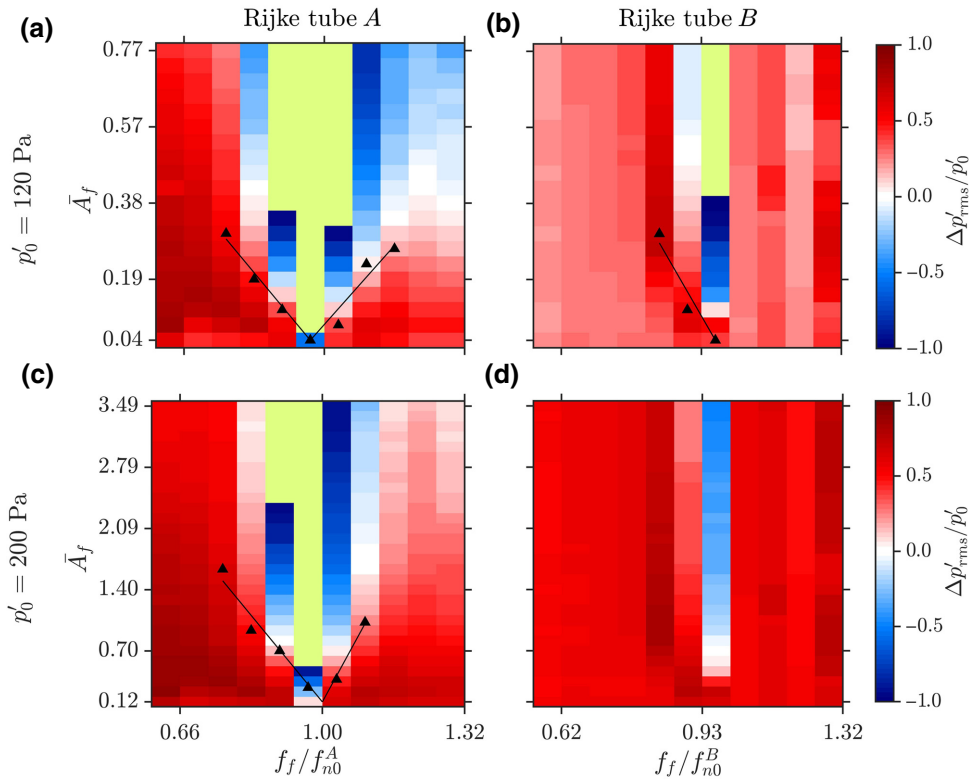
FIG. 7. The amplitude and phase response (black lines) of Rijke tubes A and B when coupled nonidentical oscillators are subjected to asymmetric forcing for (a),(b) $p_0' = 120$ Pa and (c),(d) $p_0' = 200$ Pa. The effect of forcing is less effective in synchronizing and quenching of LCOs in Rijke tube B, while it shows regions of forced synchronization and quenching of LCOs in Rijke tube A. Inside the region marked in green, $\Delta p_{\text{rms}}'/p_0'$ varies in the range $(-6.03, -1)$ in (a), $(-1.47, -1)$ in (b), and $(-3.04, -1)$ in (c). The common parameters in all the plots are $\Delta f_{n0} = 10$ Hz, $L = 105$ cm, $d = 1$ cm.

over which Rijke tube B is synchronized to forcing for $p_0' = 120$ Pa [Fig. 7(b)]. The region of forced synchronization is completely absent when p_0' is increased to 200 Pa [Fig. 7(d)]. In contrast, as the external forcing is applied directly to Rijke tube A, it is easily synchronized with the forcing, as seen from the longer boundaries of the Arnold tongue for both $p_0' = 120$ and 200 Pa in Figs. 7(a) and 7(c), respectively.

Finally, the mechanism through which forced synchronization is attained for $p_0' = 120$ Pa in the nonidentical system is quite different from that of the coupled system. As the forcing amplitude is increased, the oscillator that is subjected to external forcing (i.e., Rijke tube A) synchronizes with the forcing signal first, followed by the forced synchronization of the entire system, i.e., the coupled system of Rijke tubes A and B. The entire system undergoes forced synchronization only in the $f_f/f_{n0}^{A,B} < 1$ range. The transition from desynchronization to forced synchronization for Rijke tube A takes place through the following sequence of bifurcations: (i) from desynchronized two-frequency quasiperiodicity (f_{n0}^A, f_{n0}^B) to three-frequency quasiperiodicity $(f_{n0}^A, f_{n0}^B, f_f)$ as A_f is increased, and (ii) from three-frequency quasiperiodicity to synchronized limit cycle (f_f).

This route was reported for coupled Van der Pol oscillators under asymmetric forcing [19,20]. However, Rijke tube B goes from two-frequency quasiperiodicity (f_{n0}^A, f_{n0}^B) to synchronized limit cycle (f_f) when $f_f/f_{n0} < 1$ for $p_0' = 120$ Pa. For $p_0' = 200$ Pa, the acoustic pressure fluctuations in Rijke tube B remain desynchronized with the forcing signal throughout the $\bar{A}_f$-f_f parameter plane.

The amplitude response of Rijke tubes A and B shows that the significant suppression of LCOs can still be achieved at nonresonant conditions (i.e., $|f_f \ll f_{n0}|$) of forcing. The region of resonant amplification observed around $f_f/f_{n0} \sim 1$ is very small for Rijke tube B as compared to Rijke tube A. Furthermore, the comparison of the forced response of the coupled oscillators with $p_0' = 120$ Pa [Figs. 7(a) and 7(b)] and $p_0' = 200$ Pa [Figs. 7(c) and 7(d)] shows that, for the higher-amplitude LCOs, we need significantly larger values of $\bar{A}_f$ for synchronization and quenching of oscillations in both the Rijke tubes. This is similar to the observations made for identical oscillators in Fig. 6. Note that the ordinate in Figs. 7(c) and 7(d) is much larger than that in Figs. 7(a) and 7(b). Thus, we reemphasize that the effect of forcing is more significant in suppressing LCOs in both coupled thermoacoustic oscillators

if their natural frequencies are nearly the same as compared to that seen in the case of nonidentical oscillators.

IV. MATHEMATICAL MODEL

In this section, we develop a reduced-order model for the system of coupled horizontal Rijke tubes subjected to asymmetric forcing. The model of the uncoupled oscillator is based on Ref. [36]. We neglect the effects of mean flow and mean temperature gradient in the duct. The temporal evolution of a single Rijke tube is described by the set of ordinary differential equations (ODEs)

$$\frac{d\eta_j}{dt} = \dot{\eta}_j, \qquad (2)$$

$$\frac{d\dot{\eta}_j}{dt} + 2\xi_j \omega_j \dot{\eta}_j + k_j^2 \eta_j$$
$$= -j\pi K\left[\sqrt{\left|\frac{1}{3} + u_f'(t-\tau)\right|} - \sqrt{\frac{1}{3}}\right]\sin(j\pi x_f), \quad (3)$$

where $k_j = j\pi$ refers to the nondimensional wave number and $\omega_j = j\pi$ refers to the nondimensional angular frequency of the jth mode. Other parameters are the nondimensional heater power K and nondimensional velocity u_f' at the nondimensional heater location x_f. The heat release rate is modeled using a modified form of King's law [37,38] that correlates the quasisteady heat transfer from a heated cylinder to the flow around it. The thermal inertia of the heat transfer in the medium is captured by a time lag parameter τ. The coefficient ξ_j appearing in the second term of Eq. (3) represents the frequency-dependent damping [39], and is given by the ansatz [40]

$$\xi_j = \frac{c_1 \omega_j/\omega_1 + c_2\sqrt{\omega_1/\omega_j}}{2\pi}, \qquad (4)$$

where c_1 and c_2 are the damping coefficients that determine the amount of damping. We choose the values $c_1 = 0.1$ and $c_2 = 0.06$ based on Ref. [40] for all the simulations. We also set $x_f = 0.25 (= L/4)$, as it is the most favorable location for the onset of thermoacoustic instability [39]. The nondimensional velocity u' and nondimensional pressure p' fluctuations in the model are written in terms of the Galerkin modes [41]:

$$p'(x,t) = -\sum_{j=1}^{N} \frac{\gamma M}{j\pi}\dot{\eta}_j(t)\sin(j\pi x), \qquad (5)$$

$$u'(x,t) = \sum_{j=1}^{N} \eta_j(t)\cos(j\pi x). \qquad (6)$$

For Rijke tubes, Matveev [39] and Sayadi *et al.* [42] have shown that the first mode is the most unstable of all the

other modes. Consequently, we consider only the first mode ($N = 1$) in our numerical analysis, to keep the model simple.

Let the superscripts "a" and "b" denote Rijke tubes A and B, respectively. We assume that the two Rijke tubes are coupled through time-delay and dissipative couplings. The governing equations for Rijke tube A in a system of coupled nonidentical Rijke tubes with asymmetric sinusoidal forcing can then be written as

$$\frac{d\eta_j^a}{dt} = \dot{\eta}_j^a, \qquad (7)$$

$$\frac{d\dot{\eta}_j^a}{dt} + 2\xi_j\left(\frac{\omega_j}{r^a}\right)\dot{\eta}_j^a + \left(\frac{k_j}{r^a}\right)^2 \eta_j^a$$
$$= -\frac{j\pi}{(r^a)^2}K\left[\sqrt{\left|\frac{1}{3} + u_f'^a(t-\tau)\right|} - \sqrt{\frac{1}{3}}\right]\sin\left(\frac{j\pi x_f}{r^a}\right)$$
$$+ \underbrace{K_d(\dot{\eta}_j^b - \dot{\eta}_j^a)}_{\text{dissipative coupling}} + \underbrace{K_\tau(\dot{\eta}_j^b(t-\tau_{\text{tube}}) - \dot{\eta}_j^a(t))}_{\text{time-delay coupling}}$$
$$+ \underbrace{[A_f \sin(2\pi f_f t)]^a}_{\text{forcing term}}, \qquad (8)$$

where r^a is defined as the ratio of the length of the duct to a reference length, L_a/L_{ref}. We consider L_a to be the reference length. The governing equations for Rijke tube B can be obtained by changing the superscripts "a" to "b", and vice-versa, in Eqs. (7) and (8). For identical oscillators, $r^a = r^b = 1$. For nonidentical oscillators, $r^a = 1$ and $r^b = L_b/L_a = \omega_a/\omega_b$. The detailed derivation of Eq. (8) is provided in Sec. IV of the Supplemental Material [34].

The second and third terms on the right-hand side of Eq. (8) are the dissipative and time-delay coupling terms, respectively. Dissipative coupling encapsulates the interaction that arises from the mass transfer between the two ducts [35]. Time-delay coupling quantifies the time taken by acoustic waves to propagate through the coupling tube connecting the two Rijke tubes [4,23]. Thus, τ_{tube} denotes the time delay in the response induced by one Rijke tube on the other, and is proportional to the length of the coupling tube, i.e., $\tau_{\text{tube}} \propto L/c$, where c is the speed of sound inside the coupling tube. The fourth term is the sinusoidal forcing term with amplitude A_f and frequency f_f. The external forcing is applied only to Rijke tube A.

The effect of the source term is characterized by the time delay τ, which captures the thermal inertia of the heat transfer in the medium. The ODEs given in Eqs. (7) and (8) are solved numerically using dde23, an inbuilt function for solving delay differential equations in MATLAB® [43], and p' is calculated using Eq. (5). The parameters that are kept constant during the simulations are indicated in Table I. These parameters have been chosen such that both

TABLE I. Model parameters kept constant throughout the numerical analysis of the reduced-order model.

Parameter	Value	Parameter	Value	Parameter	Value
N	1	τ	0.25	K	5
γ	1.4	M	0.005	x_f	0.25
c_1	0.1	c_2	0.06	ω_f	$j\pi$

the oscillators exhibit limit-cycle oscillations at a parametric location away from the bistable regime and also to quantitatively match the experimental results.

A. Model results for a single oscillator and mutually coupled oscillators

We begin by analyzing the forced response of a single Rijke tube by adding the forcing term $A_f \sin(2\pi f_f t)$ to the right-hand side of Eq. (3). Considering only the first mode, we get the set of ODEs

$$\frac{d\eta_1}{dt} = \dot{\eta}_1, \tag{9}$$

$$\frac{d\dot{\eta}_1}{dt} + 2\xi_1\omega_1\dot{\eta}_1 + k_1^2\eta_1$$
$$= -\pi K\left[\sqrt{\left|\frac{1}{3} + u_f'(t-\tau)\right|} - \sqrt{\frac{1}{3}}\right]\sin(\pi x_f)$$
$$+ \underbrace{A_f \sin(2\pi f_f t)}_{\text{forcing term}}. \tag{10}$$

In Fig. 8 we show the two-parameter bifurcation plot in the A_f-f_f plane, illustrating the phase and amplitude

dynamics of the limit-cycle oscillations in a single Rijke tube, obtained from the mathematical model. We observe the existence of Arnold tongue in Fig. 8(a) along with the region of asynchronous quenching ($\Delta p'_{\text{rms}}/p_0' > 0.5$) in Fig. 8(b). We observe the qualitative match between experimental results shown in Fig. 2 and those obtained from the model in Fig. 8. However, there are a number of differences. First, the region of asynchronous quenching observed in the model is smaller than that observed in the experiments. Second, the resonant amplification region is spread over a larger extent of parameter values in the model. Finally, the Arnold tongue obtained from the model is symmetrical as opposed to left skewed in the experiments. The skewness of the Arnold tongue increases as the model heater power K is increased to higher values, indicating the nonlinear behavior of the overall systems. Figure 8 has been shown for a model heater power K for which we get the best match with the experimental results in Fig. 2.

In Fig. 3, we showed that the state of AD is attained in coupled Rijke tubes only when there is a frequency detuning present in the two oscillators, in addition to the dissipative and time-delay coupling due to the connecting tube. In Fig. 9, we show the effect of coupling and frequency detuning on the occurrence of the state of AD in the model. We fix the values of $K_d = 1.0$ and $K_\tau = 0.2$ in Eq. (8), and vary τ_{tube} and the frequency detuning Δf_{n0}. For identical oscillators ($\Delta f_{n0} = 0$), we do not observe any appreciable reduction in the amplitude of the LCOs. However, for a finite value of detuning, we observe the state of AD in the model, consistent with our experimental observations in Fig. 3. Thus, the effect of changing the length of the coupling tube is captured quite well by the time delay τ_{tube}.
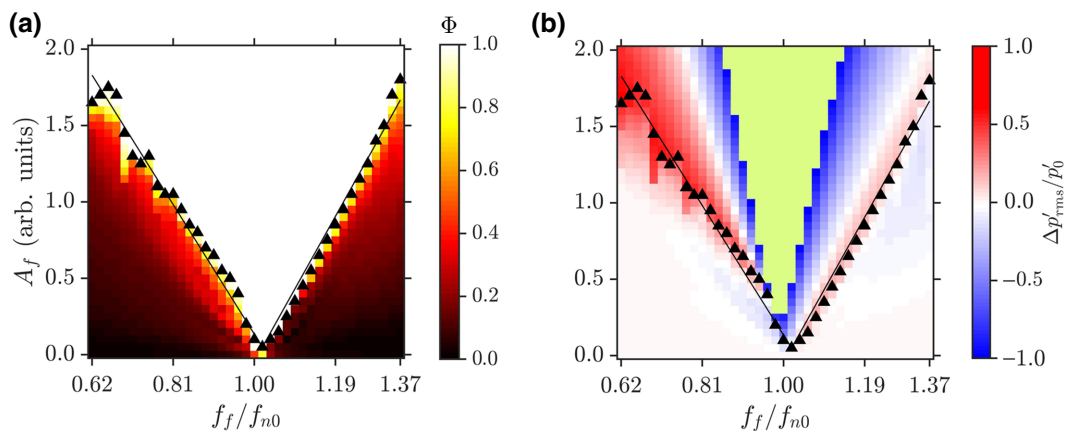

FIG. 8.   (a) The phase response and (b) the amplitude response obtained from the model of a single Rijke tube under external forcing. The synchronization boundaries are obtained through a least-square fit of points where $\Phi = 0.98$. The Arnold tongue and extent of asynchronous quenching from the model show a qualitative match with the experimental results in Fig. 2. In (b), the green region around $f_f/f_{n0} = 1$ indicates the increase of LCO amplitude above twice of its unforced value, where $\Delta p'_{\text{rms}}/p_0'$ varies in the range $(-6.35, -1)$.
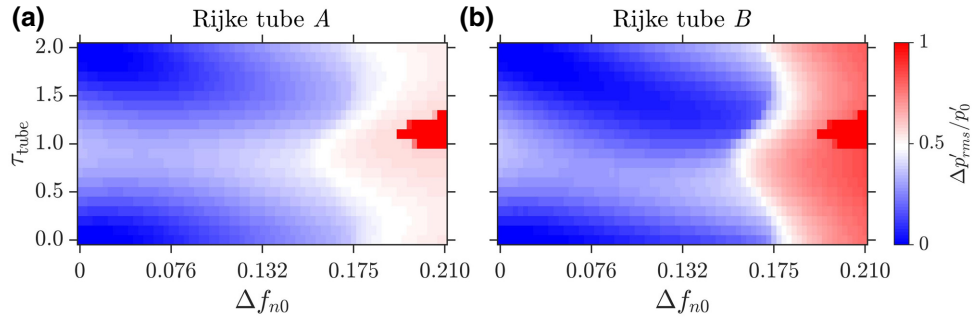
FIG. 9. Two-parameter bifurcation plots between the frequency detuning (Δf_{n0}) between the two Rijke tube oscillators and the coupling delay (τ_{tube}). We keep K_d and K_τ constant at 1.0 and 0.2, respectively. The dark red regions in the plots represent regions of AD. At other places, LCOs are observed at reduced amplitude due to coupling.

The results summarized in Figs. 8 and 9 validate our model against experimental observations for a single Rijke tube and coupled Rijke tubes reported in the present study (Figs. 2 and 3), as well as those made in past studies [23, 25,44]. We now turn our attention towards modeling the effect of asymmetric forcing on the coupled Rijke tubes.

B. Model results for coupled behavior of thermoacoustic oscillators under asymmetric forcing

In Fig. 10, we plot the amplitude and the phase response of the coupled identical Rijke tubes under asymmetric forcing, i.e., only Rijke tube A is subjected to external forcing according to Eq. (8). The effect of coupling is parameterized by τ_{tube}, while that of external forcing by

A_f. The forcing frequency is fixed at $f_f/f_{n0} = 0.6$. The values of K_d, K_τ, and K are fixed at 1.0, 0.2, and 5.0, respectively. Note that the heater power $K = 5.0$ leads to high-amplitude LCOs in the two Rijke tubes ($p_0'^{A,B} = 648$ Pa).

For $A_f = 0$, we note that the change in τ_{tube} leads to very low suppression in either of the oscillators ($\Delta p_{\text{rms}}'/p_0' < 0.5$). This is again a reflection of the fact that AD is not possible when identical oscillators are coupled, as seen in the experimental results of Fig. 3. Our aim is to illustrate that external forcing can lead to significant quenching of LCOs in the identical oscillators. When A_f is increased, we observe a decrease in the amplitude of LCOs in both the oscillators after a critical value of A_f. The effect of forcing is more pronounced in Rijke tube B compared to that in
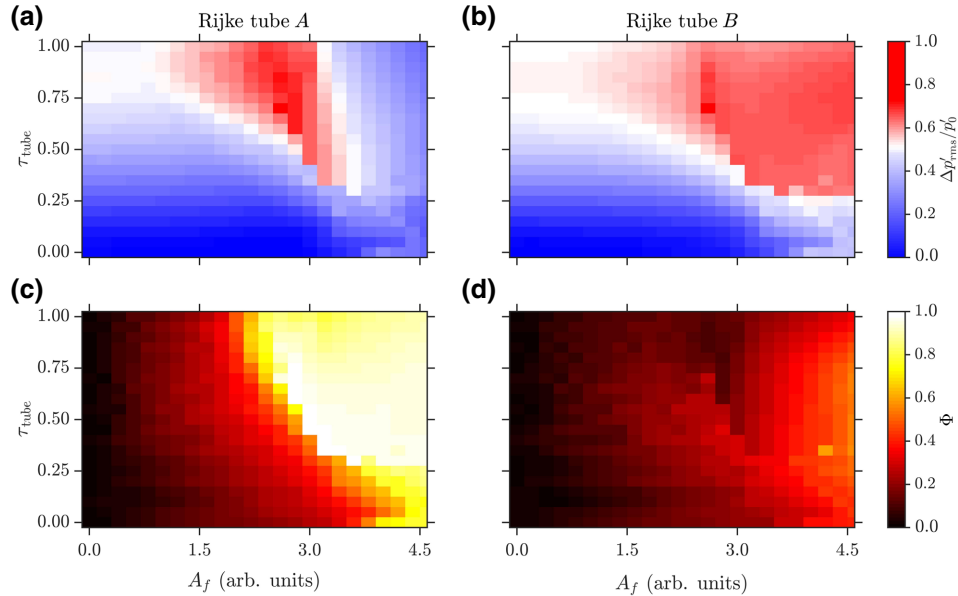

FIG. 10. (a),(b) Amplitude and (c),(d) phase response of coupled identical oscillators under asymmetric forcing for different values of τ_{tube} and A_f. The amplitude response is indicated by the fractional change in the amplitude of LCOs ($\Delta p_{\text{rms}}'/p_0'$), while the phase response is quantified by the Φ between p' and the forcing signal. For $\tau_{\text{tube}} > 0.4$ and $A_f > 1.5$, a large suppression in the amplitude of LCOs is observed in the two Rijke tubes.

Rijke tube A, which is evident from the larger "red" region in Fig. 10(b) compared to that in Fig. 10(a).

The results obtained from the model (Fig. 10) can be compared with the experimental results shown in Fig. 5. The ratio of forcing frequency to natural frequency is kept the same for ease of comparison. Although the magnitude of amplitude suppression is not captured quantitatively by the model, the qualitative trends such as the extent of amplitude suppression in the two oscillators along with the forced synchronization characteristics are consistent between the experimental and numerical results. Compared to the pressure oscillations in Rijke tube B exhibiting complete suppression in the experimental study [e.g., point (e) in Fig. 5(a)], we observe around 70% suppression in the amplitude of LCOs in Rijke tube B.

Similar to experimental results, we also observe that the LCOs in Rijke tube B remain desynchronized with the forcing signal for a large extent of the parameter plane. The region of quenching of LCOs in Rijke tube A ($\Delta p'_{\text{rms}}/p'_0 \sim 1$) nearly coincides with the onset of forced synchronization (PLV ~ 1). The results shown in Fig. 10 are in qualitative agreement with the experimental results indicated in Figs. 5(a)–5(d).

In Fig. 11, we depict the fractional change in the amplitude of LCOs for each oscillator overlapped with the Arnold tongue in the A_f-f_f plane, obtained from the numerical simulations for the case where identical oscillators are asymmetrically forced. The values of the coupling constants are fixed at $K_d = 1.0$, $K_\tau = 0.20$, and $\tau_{\text{tube}} = 0.4$. The normalized natural frequency of both the oscillators is 0.5, and the normalized heater power is maintained at $K = 5.0$.

We see that the amplitude dynamics observed during the experiments, as depicted in Fig. 6, is well captured by the numerical model in Fig. 11. From the numerical results, we observe a larger magnitude of suppression of LCOs in Rijke tube B, compared to that in Rijke tube A. Furthermore, the high magnitude of suppression ($\Delta p'_{\text{rms}}/p'_0 > 0.5$) in Rijke tube B nearly coincides with the boundary of the Arnold tongue in Rijke tube A. The resonant synchronization region in Rijke tube B is smaller in size compared to that in Rijke tube A. The model does not adequately capture the phase dynamics observed in the experiments. Although the Arnold tongue is similar for both the Rijke tubes, the phase locking values observed prior to the onset of forced synchronization are lower in Rijke tube B than in Rijke tube A. Also, the synchronance region (shown in green) is skewed towards the left side of the $f_f/f_{n0} = 1.00$ value. This is different from the experimental results (Fig. 6), where the resonant amplification region is almost symmetrically located around the $f_f/f_{n0} = 1.00$ value.

Finally, we use our model to characterize the response of asymmetric forcing on the Arnold tongue and amplitude characteristics of coupled nonidentical Rijke tubes. The coupling constants and nondimensional heater power values are kept the same as those used to get the results shown in Fig. 11, i.e., $K_d = 1.0$, $K_\tau = 0.2$, $\tau_{\text{tube}} = 0.4$, and $K = 5$. This ensures consistency of the initial and boundary conditions, as ensured in the experiments. In Sec. III D, to study the forced response of coupled nonidentical Rijke tube oscillators, the natural frequencies of the LCOs in Rijke tubes A and B are maintained at 150 and 160 Hz, respectively, which equals a frequency ratio of $150/160 = 0.9375$. Consistent with the experiments, the value of r^b is kept as 0.9375 to analyze the reduced-order model given in Eqs. (7) and (8).

We observe that the effect of forcing is quite insignificant for forced synchronization of LCOs in Rijke tube B,
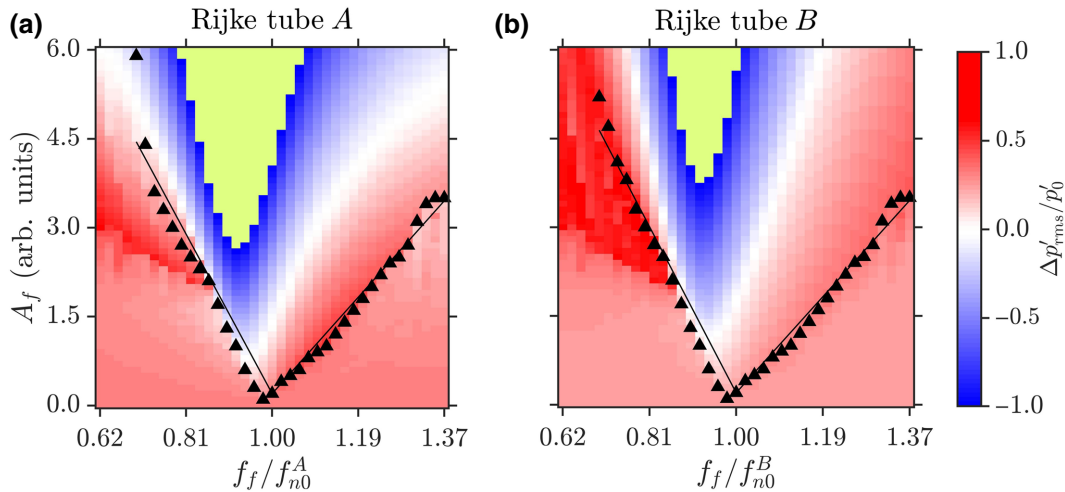

FIG. 11. The amplitude response and overlapped Arnold tongue for identical, coupled Rijke tubes from the numerical model. External forcing is applied to Rijke tube A. The synchronization boundaries are obtained through a least-square fit of points where PLV = 0.98. For the green region around $f_f/f_{n0} = 1$, values of $\Delta p'_{\text{rms}}/p'_0$ vary in the range $(-3.20, -1)$ in (a) and $(-2.08, -1)$ in (b). The coupling parameters are $K_d = 1.0$, $K_\tau = 0.2$, and $\tau_{\text{tube}} = 0.4$.
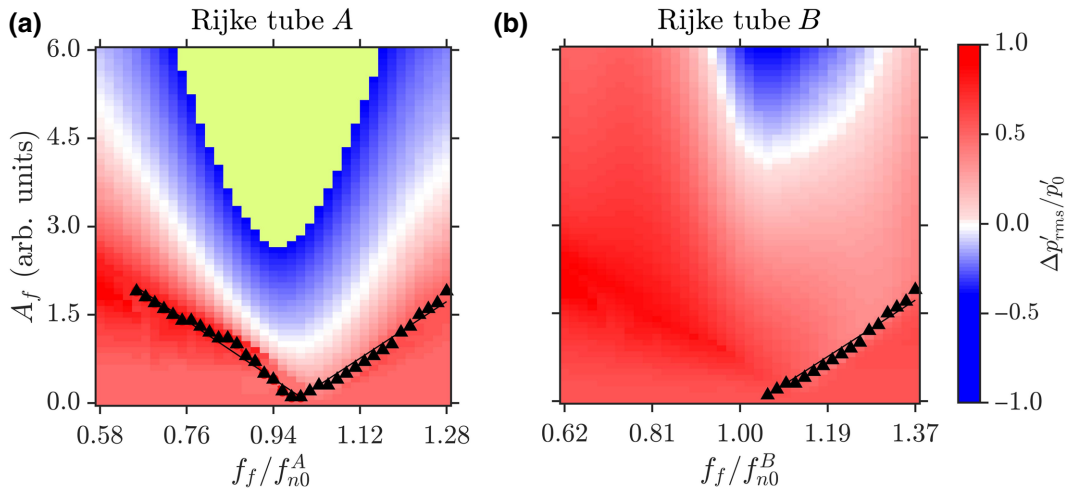
FIG. 12. The amplitude response and overlapped Arnold tongue for nonidentical, coupled Rijke tubes from the numerical model. External forcing is applied to Rijke tube A. The synchronization boundaries are obtained through a least-square fit of points where PLV $= 0.98$. Inside the green region in (a), $\Delta p'_{\mathrm{rms}}/p'_0$ varies in the $(-2.66, -1)$ range. The coupling parameters are $K_d = 1.0$, $K_\tau = 0.2$, and $\tau_{\mathrm{tube}} = 0.4$.

consistent with the experimental results (Fig. 7). A significant suppression of the amplitude of LCOs is observed at nonresonant conditions of forcing in Rijke tube A. The region of resonant amplification is absent for Rijke tube B, although we do observe amplification of the amplitude of LCOs at higher values of A_f in Fig. 12(b). Some differences are present between the experimental (Fig. 7) and numerical results (Fig. 12). First, the forced synchronization of Rijke tube B is observed for $f_f/f_{n0}^B < 1$ values during the experiments, whereas pressure oscillations in the Rijke tube B model oscillator undergo forced synchronization for $f_f/f_{n0}^B > 1$ values. Second, the Arnold tongue is spread over a larger extent of parameter values for a system of coupled nonidentical oscillators as opposed to that in a system of coupled identical oscillators (Fig. 11). During the experiments, an opposite behavior is observed in Fig. 7(c), where the size of the Arnold tongue of Rijke tube A for coupled nonidentical oscillators is less when compared to that in the coupled identical oscillators [Fig. 6(c)]. The qualitative differences between the results can be attributed to the various assumptions used while deriving the reduced-order model, such as absence of mean flow, zero temperature gradient, nonheat conducting gas, etc. A more detailed study is needed to examine the effects of such assumptions on the numerical results.

V. CONCLUSIONS

In this proof-of-concept study, we investigate the phase and the amplitude dynamics of coupled thermoacoustic oscillators under asymmetric forcing, and present a model that qualitatively captures the experimental results. In particular, we discuss the viability of simultaneous coupling

and forcing as a method for controlling thermoacoustic instability in a system of multiple combustors.

The forced response of LCOs in a single oscillator (Rijke tube) shows the presence of an Arnold tongue along with a region of asynchronous quenching for the parametric range of $f_f < f_{n0}$. The region of asynchronous quenching coincides with the boundary of forced synchronization of the acoustic pressure fluctuations in the system [16]. The presence of the Arnold tongue and asynchronous quenching are consistent with the results observed in previous studies conducted on Rijke tubes [16] and laminar combustors [31–33]. We note that the characteristics of forced synchronization of LCOs are dependent on the amplitude of LCOs in the unforced state. In particular, the region of forced synchronization (or Arnold tongue) of the oscillator gets narrower as the amplitude of LCOs is increased. In addition, the coupled response of two Rijke tube oscillators (A and B) show the occurrence of two different states of oscillation quenching, i.e., amplitude death and partial amplitude death. These states occur only when a finite frequency detuning is present between the oscillators, and the length of the coupling tube lies within a specific range.

To expand the parametric range of oscillation quenching in two mutually coupled Rijke tube oscillators, we acoustically force Rijke tube A. We observe that the suppression of LCOs in coupled identical Rijke tube oscillators is possible through the combined effect of mutual coupling and asynchronous quenching. A significantly larger value of the forcing amplitude is required to synchronize and quench the large-amplitude LCOs in the coupled thermoacoustic oscillators. This behavior is depicted through an increase in the steepness of the boundaries of the Arnold tongue as the amplitude of the LCOs is increased.

Suppression of LCOs is observed predominantly for $f_f < f_{n0}$ in Rijke tube A, while it is observed on both sides of f_{n0} in Rijke tube B. We note that external forcing widens the region of coupling and forcing parameters over which the oscillation quenching states are observed in both the oscillators than when only one of the two mechanisms of control is applied on its own. Most importantly, although Rijke tube A is forced, the suppression of LCOs is more significant in Rijke tube B in comparison with that in Rijke tube A. We also study the coupled behavior of two nonidentical thermoacoustic oscillators under asymmetric forcing. We witness that, because of the direct influence of forcing, Rijke tube A exhibits the features of forced synchronization, while Rijke tube B (not directly forced) remains desynchronized with the forcing signal. As a result, we observe a significant suppression of LCOs in Rijke tube A and not in Rijke tube B, which is opposite to the behavior of forced response of coupled identical thermoacoustic oscillators. Finally, we qualitatively capture the experimental results through a reduced-order model of two coupled Rijke tubes. Good agreement is obtained between the experimental and numerical results.

Periodic forcing thus aids mitigation of the thermoacoustic instability observed in coupled identical oscillators. We believe that the present investigation on asymmetrically forced prototypical coupled thermoacoustic oscillators could prove to be a benchmark specifically for the control of thermoacoustic oscillations observed in can combustors with multiple cans, and for coupled nonlinear oscillators subjected to external forcing in general nonlinear dynamics literature.

ACKNOWLEDGMENTS

[1] A. Jenkins, Self-oscillation, Phys. Rep. **525**, 167 (2013).

[2] S. Strogatz, *Sync: The Emerging Science of Spontaneous Order* (Penguin, UK, 2004).

[3] S. H. Strogatz, D. M. Abrams, A. McRobie, B. Eckhardt, and E. Ott, Crowd synchrony on the millennium bridge, Nature **438**, 43 (2005).

[4] T. Biwa, S. Tozuka, and T. Yazaki, Amplitude Death in Coupled Thermoacoustic Oscillators, Phys. Rev. Appl. **3**, 034006 (2015).

[5] T. C. Lieuwen and V. Yang, *Combustion Instabilities in gas Turbine Engines: Operational Experience, Fundamental Mechanisms, and Modeling* (American Institute of Aeronautics and Astronautics, Reston, VA, 2005).

[6] R. I. Sujith and V. R. Unni, Complex system approach to investigate and mitigate thermoacoustic instability in turbulent combustors, Phys. Fluids **32**, 061401 (2020).

[7] A. Pikovsky, J. Kurths, M. Rosenblum, and J. Kurths, *Synchronization: A Universal Concept in Nonlinear Sciences* (Cambridge University Press, Cambridge, England, 2003), Vol. 12.

[8] M. P. Juniper and R. I. Sujith, Sensitivity and nonlinearity of thermoacoustic oscillations, Annu. Rev. Fluid Mech. **50**, 661 (2018).

[9] K. Pyragas, F. Lange, T. Letz, J. Parisi, and A. Kittel, Stabilization of an unstable steady state in intracavity frequency-doubled lasers, Phys. Rev. E **61**, 3721 (2000).

[10] A. Kumar, S. Cardanobile, S. Rotter, and A. Aertsen, The role of inhibition in generating and controlling parkinson's disease oscillations in the basal ganglia, Front. Syst. Neurosci. **5**, 86 (2011).

[11] S. R. Huddy and J. D. Skufca, Amplitude death solutions for stabilization of dc microgrids with instantaneous constant-power loads, IEEE Trans. Power Electron. **28**, 247 (2012).

[12] R. E. Mirollo and S. H. Strogatz, Amplitude death in an array of limit-cycle oscillators, J. Stat. Phys. **60**, 245 (1990).

[13] F. M. Atay, Total and partial amplitude death in networks of diffusively coupled oscillators, Phys. D: Nonlinear Phenom. **183**, 1 (2003).

[14] A. Balanov, N. Janson, D. Postnov, and O. Sosnovtseva, *Synchronization: From Simple to Complex* (Springer Science & Business Media, Berlin, 2008).

[15] B. Keen and W. Fletcher, Suppression of a Plasma Instability by the Method of 'Asynchronous Quenching', Phys. Rev. Lett. **24**, 130 (1970).

[16] S. Mondal, S. A. Pawar, and R. I. Sujith, Forced synchronization and asynchronous quenching of periodic oscillations in a thermoacoustic system, J. Fluid Mech. **864**, 73 (2019).

[17] P. M. Battelino, Persistence of three-frequency quasiperiodicity under large perturbations, Phys. Rev. A **38**, 1495 (1988).

[18] V. S. Anishchenko, S. V. Astakhov, T. E. Vadivasova, and A. V. Feoktistov, Numerical and experimental study of external synchronization of two-frequency oscillations, Nelineinaya Dinamika [Russ. J. Nonlinear Dyn.] **5**, 237 (2009).

[19] V. Anishchenko, S. Astakhov, and T. Vadivasova, Phase dynamics of two coupled oscillators under external periodic force, EPL (Europhys. Lett.) **86**, 30003 (2009).

[20] V. Anishchenko, S. Nikolaev, and J. Kurths, Bifurcational mechanisms of synchronization of a resonant limit cycle on a two-dimensional torus, Chaos: Interdisc. J. Nonlinear Sci. **18**, 037123 (2008).

[21] X. Wei, M. Randrianandrasana, M. Ward, and D. Lowe, Nonlinear dynamics of a periodically driven duffing resonator coupled to a Van der Pol oscillator, Math. Problems Eng. **2011**, 1 (2011).

[22] J. Honerkamp, The heart as a system of coupled nonlinear oscillators, J. Math. Biol. **18**, 69 (1983).

[23] N. Thomas, S. Mondal, S. A. Pawar, and R. I. Sujith, Effect of time-delay and dissipative coupling on amplitude death in coupled thermoacoustic oscillators, Chaos: Interdiscip. J. Nonlinear Sci. **28**, 033119 (2018).

[24] N. Thomas, S. Mondal, S. A. Pawar, and R. I. Sujith, Effect of noise amplification during the transition to amplitude death in coupled thermoacoustic oscillators, Chaos: Interdiscip. J. Nonlinear Sci. **28**, 093116 (2018).

[25] S. Dange, K. Manoj, S. Banerjee, S. A. Pawar, S. Mondal, and R. I. Sujith, Oscillation quenching and phase-flip bifurcation in coupled thermoacoustic systems, Chaos: Interdiscip. J. Nonlinear Sci. **29**, 093135 (2019).

[26] H. Hyodo, M. Iwasaki, and T. Biwa, Suppression of Rijke tube oscillations by delay coupling, J. Appl. Phys. **128**, 094902 (2020).

[27] H. Jegal, K. Moon, J. Gu, L. K. Li, and K. T. Kim, Mutual synchronization of two lean-premixed gas turbine combustors: Phase locking and amplitude death, Combust. Flame **206**, 424 (2019).

[28] K. Moon, Y. Guan, L. K. Li, and K. T. Kim, Mutual synchronization of two flame-driven thermoacoustic oscillators: Dissipative and time-delayed coupling effects, Chaos: Interdiscip. J. Nonlinear Sci. **30**, 023110 (2020).

[29] S. Balusamy, L. K. Li, Z. Han, M. P. Juniper, and S. Hochgreb, Nonlinear dynamics of a self-excited thermoacoustic system subjected to acoustic forcing, Proc. Combust. Inst. **35**, 3229 (2015).

[30] K. Kashinath, L. K. Li, and M. P. Juniper, Forced synchronization of periodic and aperiodic thermoacoustic oscillations: Lock-in, bifurcations and open-loop control, J. Fluid Mech. **838**, 690 (2018).

[31] Y. Guan, V. Gupta, K. Kashinath, and L. K. Li, Open-loop control of periodic thermoacoustic oscillations: Experiments and low-order modelling in a synchronization framework, Proc. Combust. Inst. **37**, 5315 (2019).

[32] A. Roy, S. Mondal, S. A. Pawar, and R. I. Sujith, On the mechanism of open-loop control of thermoacoustic instability in a laminar premixed combustor, J. Fluid Mech. **884**, A2 (2020).

[33] Y. Guan, V. Gupta, M. Wan, and L. K. Li, Forced synchronization of quasiperiodic oscillations in a thermoacoustic system, J. Fluid Mech. **879**, 390 (2019).

[34] See Supplemental Material at http://link.aps.org/supplemental/10.1103/PhysRevApplied.15.044011 for R^2 values of least-square fitted lines, dynamics of period-3 oscillations, effects of varying coupling tube parameters, and a detailed derivation of the mathematical model of coupled Rijke tubes.

[35] K. Bar-Eli, On the stability of coupled chemical oscillators, Phys. D: Nonlinear Phenom. **14**, 242 (1985).

[36] K. Balasubramanian and R. Sujith, Thermoacoustic instability in a Rijke tube: Non-normality and nonlinearity, Phys. Fluids **20**, 044103 (2008).

[37] L. V. King, XII. On the convection of heat from small cylinders in a stream of fluid: Determination of the convection constants of small platinum wires with applications to hot-wire anemometry, Philos. Trans. R. Soc. London. Ser. A, Containing Papers Math. Phys. Charact. **214**, 373 (1914).

[38] M. A. Heckl, Non-linear acoustic effects in the Rijke tube, Acta Acust. United Acust. **72**, 63 (1990).

[39] K. I. Matveev, Ph.D. thesis, California Institute of Technology, 2003.

[40] J. Sterling and E. Zukoski, Nonlinear dynamics of laboratory combustor pressure oscillations, Combust. Sci. Technol. **77**, 225 (1991).

[41] M. E. Lores and B. T. Zinn, Nonlinear longitudinal combustion instability in rocket motors, Combust. Sci. Technol. **7**, 245 (1973).

[42] T. Sayadi, V. L. Chenadec, P. Schmid, F. Richecoeur, and M. Massot, Thermoacoustic instability- a dynamical system and time domain analysis, arXiv:1312.3101 (2013).

[43] L. F. Shampine and S. Thompson, Solving DDEs in Matlab, Appl. Numer. Math. **37**, 441 (2001).

[44] H. Hyodo and T. Biwa, Stabilization of thermoacoustic oscillators by delay coupling, Phys. Rev. E **98**, 052223 (2018).